Properties of iron sulfide, hydrosulfide, and mixed sulfide/hydrosulfide cluster anions through photoelectron spectroscopy and density functional theory calculations

Shi Yin and Elliot R. Bernstein

Citation: The Journal of Chemical Physics **145**, 154302 (2016); doi: 10.1063/1.4964651
View online: http://dx.doi.org/10.1063/1.4964651
View Table of Contents: http://aip.scitation.org/toc/jcp/145/15
Published by the American Institute of Physics

Properties of iron sulfide, hydrosulfide, and mixed sulfide/hydrosulfide cluster anions through photoelectron spectroscopy and density functional theory calculations

Shi Yin and Elliot R. Bernstein[a)]
Department of Chemistry, NSF ERC for Extreme Ultraviolet Science and Technology, Colorado State University, Fort Collins, Colorado 80523, USA

(Received 25 August 2016; accepted 28 September 2016; published online 18 October 2016)

A new magnetic-bottle time-of-flight photoelectron spectroscopy (PES) apparatus is constructed in our laboratory. The PES spectra of iron sulfide, hydrosulfide, and mixed sulfide/hydrosulfide [$FeS_m(SH)_n^-$; m, n = 0–3, $0 < (m + n) \leq 3$] cluster anions, obtained at 2.331 eV (532 nm) and 3.492 eV (355 nm) photon energies, are reported. The electronic structure and bonding properties of these clusters are additionally investigated at different levels of density functional theory. The most probable structures and ground state spin multiplicity for these cluster anions are tentatively assigned by comparing their theoretical first vertical detachment energies (VDEs) with their respective experiment values. The behavior of S and (SH) as ligands in these iron sulfide, hydrosulfide, and mixed sulfide/hydrosulfide cluster anions is investigated and compared. The experimental first VDEs for $Fe(SH)_{1-3}^-$ cluster anions are lower than those found for their respective FeS_{1-3}^- cluster anions. The experimental first VDEs for FeS_{1-3}^- clusters are observed to increase for the first two S atoms bound to Fe^-; however, due to the formation of an S–S bond for the FeS_3^- cluster, its first VDE is found to be ~0.41 eV lower than the first VDE for the FeS_2^- cluster. The first VDEs of $Fe(SH)_{1-3}^-$ cluster anions are observed to increase with the increasing numbers of SH groups. The calculated partial charges of the Fe atom for ground state FeS_{1-3}^- and $Fe(SH)_{1-3}^-$ clusters are apparently related to and correlated with their determined first VDEs. The higher first VDE is correlated with a higher, more positive partial charge for the Fe atom of these cluster anions. Iron sulfide/hydrosulfide mixed cluster anions are also explored in this work: the first VDE for $FeS(SH)^-$ is lower than that for FeS_2^-, but higher than that for $Fe(SH)_2^-$; the first VDEs for $FeS_2(SH)^-$ and $FeS(SH)_2^-$ are close to that for FeS_3^-, but higher than that for $Fe(SH)_3^-$. The first VDEs of general iron sulfide, hydrosulfide, and mixed sulfide/hydrosulfide clusters [$FeS_m(SH)_n^-$; m, n = 0–3, $0 < (m + n) \leq 3$] are dependent on three properties of these anions: 1. the partial charge on the Fe atom, 2. disulfide bond formation (S–S) in the cluster, and 3. the number of hydrosulfide ligands in the cluster. The higher the partial charge on the Fe atom of these clusters, the larger the first VDE; however, cluster S–S bonding and more (SH) ligands in the cluster lower the cluster anion first VDE. *Published by AIP Publishing.* [http://dx.doi.org/10.1063/1.4964651]

I. INTRODUCTION

Interest in iron sulfur clusters is partially driven by their role as active centers of proteins,[1,2] and their great significance in both industrial and biochemical catalysis.[3–6] Iron sulfur clusters are ubiquitous in biology,[7] as has been recognized for many decades. Understanding of the iron sulfur system grows with continuing and expanding investigations. Iron sulfur clusters play critical roles in the active sites of a wide variety of metalloproteins and metalloenzymes, which are involved in biological electron transfer processes,[8] small molecule activation,[9–11] radical based catalytic transformations,[12] DNA repair,[13] and signal transduction.[14] Hydrogen is the most widely distributed element in the world, and it is also the most abound element in biological systems. Among various aspects of metalloprotein structure, reorganization of metal ligand(s) and/or hydrogen bonding networks around redox-active sites is often utilized in modulating natural redox potentials and functionalities.[15–18]

Action of sulfhydryl (SH) reagents on enzymes is varied and complex: most of these reactions produce conformational alterations in the enzyme involving the iron-sulfur centers.[19] The presence of (SH) groups, which is essential for catalytic activity in dehydrogenase, has been discovered in recent decades and has since been widely studied.[20–23] Direct evidence for (SH) groups activating enzymes, and the important role they play for enzyme function, has been reported recently.[24–26]

Therefore, investigations of iron–sulfur systems, ranging from bare Fe–S clusters to analogue complexes and proteins, are common throughout bioinorganic chemistry.[1] Iron sulfur clusters and complexes have been synthesized and characterized, forming a large class of organometallic chemistry.[27] A number of studies have been performed on gas phase cationic,[28,29] neutral,[30,31] and anionic[32–39]

a)Author to whom correspondence should be addressed. Electronic mail: erb@lamar.colostate.edu.

iron sulfur clusters for investigation of their composition, stability, structure, and reactivity. For example, the study of cationic iron-sulfur clusters generated by the reaction of Fe_n^+ with COS and CS_2 has been reported.[28] For products, such as $Fe_2S_2^+$, $Fe_3S_2^+$, and $Fe_4S_4^+$, the sulfur atoms are suggested to occupy different coordination sites, such as those related to analogous iron-sulfur centers identified for proteins and enzymes. Neutral iron-sulfur clusters have been observed as a reaction product of Fe_n and H_2S.[30] Our previous studies of neutral Fe_mS_n clusters suggest that the Fe_2S_2 cluster has a high catalytic activity for hydrogenation reactions of CO to form formaldehyde and methanol.[31] Fe_nS_n (n = 2, 4, and 6) neutral clusters are nitrogen fixation or other electron transfer centers in many metal–sulfur proteins, and are also observed in gas phase: anionic clusters of these compositions are also stable in supersonic jet expansions. Zhai *et al.* reported a photoelectron spectroscopic investigation of a series of anionic monoiron-sulfur clusters FeS_n^- (n = 1-6) and proposed a general structural evolution scheme on the basis of their electron binding energy trend.[32] The electronic structure and reactivity of anionic $Fe_nS_m^-$ (n = 1-8, m = 2-6) clusters were investigated using different photon energies.[33] The results imply that their corresponding neutral Fe_nS_m clusters have an alternating bonding structure between Fe and S atoms (–S–Fe–S–Fe–S–, as suggested for active sites of iron-sulfur proteins), and that their electron affinities greatly change at compositions $n = m$. Furthermore, the collision-induced dissociation (CID) of anionic iron–sulfur clusters ($Fe_nS_m^-$)[39] has shown that iron–sulfur cluster ions have interesting mass distribution and unique structural characteristics. For anionic FeS_6^- and FeS_7^- clusters, loss of neutral S_2 fragments is observed as a major dissociation channel. Extensive theoretical efforts devoted to the structural evolution of electronic properties of iron-sulfur complexes have also appeared.[40–44]

Although a broad range of both neutral and anionic iron sulfur, hydrosulfide, and mixed iron sulfur/hydrosulfide clusters has been widely studied, experimental investigation of iron hydrosulfide containing cluster anions has not been reported to the best of our knowledge. In this paper, we present a photoelectron spectroscopy (PES) study of a series of iron sulfide, hydrosulfide, and mixed sulfide/hydrosulfide cluster anions [$FeS_m(SH)_n^-$; m, n = 0–3, $0 < (m + n) \leq 3$], employing a newly constructed magnetic-bottle time-of-flight (MBTOF) photoelectron spectroscopy (PES) apparatus. The PES spectra of these cluster anions at 532 nm and 355 nm photon energies are reported, and the structural and bonding properties of these cluster anions are investigated at different theoretical levels by Density Functional Theory (DFT). The most probable structures and ground state spin multiplicities of these small, neutral, and anionic cluster series are tentatively assigned by comparing the theoretical first vertical detachment energies (VDEs) with their experiment values. A comparison of S and (SH) as ligands in these $FeS_m(SH)_n^-$ (m, n = 0–3, $0 < (m + n) \leq 3$) cluster anions are also explored both experimentally and theoretically. Values for the electron affinities of their neutral counterparts are presented and analyzed as well.

II. METHODS

A. Experimental methods

Figure 1 shows a schematic view of our MBTOF-PES apparatus. It consists of a laser vaporization cluster/molecular source, an orthogonal acceleration/extraction reflectron time of flight (oaRETOF) mass spectrometer (MS), a mass gate, a momentum decelerator, and a MBTOF electron analyzer. The cluster source and the TOFMS system are similar to ones used previously in our study of reactions of neutral metal oxide/sulfide clusters.[31,45–48] In this latter work, a Fe foil target is laser-vaporized by a 10 Hz, focused, 532 nm Nd^{3+}:YAG laser (Nd^{3+}: yttrium aluminum garnet) in the presence of a 1% H_2S in helium carrier gas, which is pulsed into the vacuum by a supersonic nozzle (R. M. Jordan, Co.) with a backing pressure of typically 100 psi. The distribution of generated iron sulfide, hydrosulfide, and mixed sulfide/hydrosulfide cluster anions is found to be a function of the ablation laser (532 nm) energy. Using

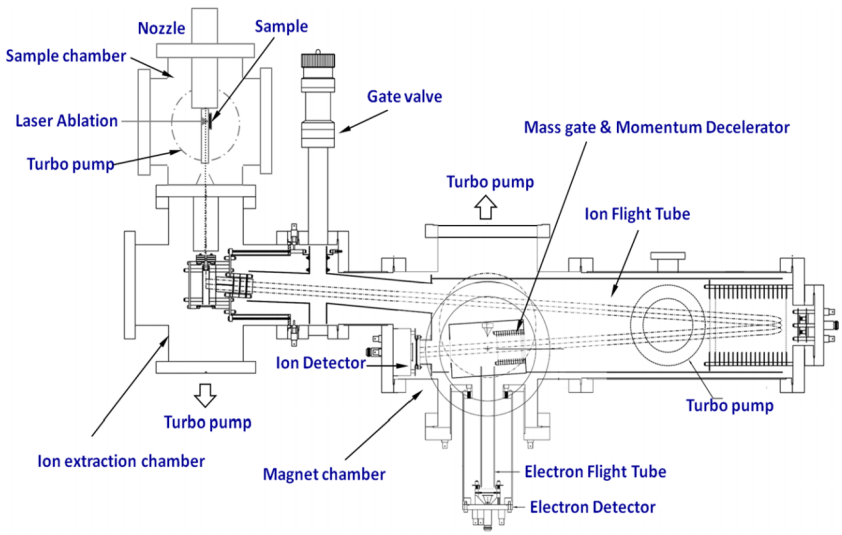

FIG. 1. Schematic view of the laser-vaporization/magnetic-bottle photoelectron spectroscopy (PES) apparatus.

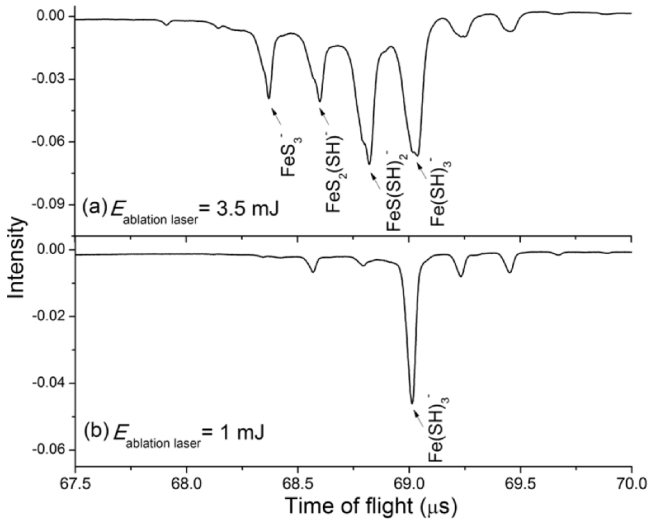

FIG. 2. Mass spectra of $FeS_m(SH)_n^-$ (m + n = 3) cluster anions obtained at (a) 3.5 mJ/pulse and (b) 1 mJ/pulse (532 nm) ablation laser energies. Note that isotopic contamination exists in the experiments. For example, the mass peak of $^{54}Fe(SH)_3^-$ is overlapped with that of $^{56}FeS_2\ (SH)^-$; however, the photoelectron spectrum feature (intense peak at ~2.17 eV) of $Fe(SH)_3^-$ is not obviously observed in the photoelectron spectrum of $FeS_2(SH)^-$ (Figure 6(b)), and also the natural abundance of ^{54}Fe is low (~5.8%), so isotopic contamination should be negligible in the experimental data.

low ablation laser energy (~1 mJ/pulse), iron hydrosulfide clusters are obtained. To generate iron sulfide and mixed sulfide/hydrosulfide cluster, high ablation laser energy (~3.5 mJ/pulse) is required. For example, the mass spectra shown in Figure 2 for $Fe(SH)_3^-$ cluster anions are generated at ~1 mJ/pulse ablation laser energy, while $FeS(SH)_2^-$, $FeS_2(SH)^-$, and FeS_3^- cluster anions appear as ablation laser energy is increased to ~3.5 mJ/pulse. Clusters generated at different ablation laser energies may well have different temperatures: typically, higher ablation laser energy will generate higher temperature clusters. In this work, photoelectron spectra of iron hydrosulfide cluster anions are obtained at a low ablation laser energy (~1 mJ/pulse), and the photoelectron spectra of iron sulfide and mixed sulfide/hydrosulfide cluster anions are obtained at a high ablation laser energy (~3.5 mJ/pulse).

Various iron sulfide, hydrosulfide, and mixed sulfide/hydrosulfide clusters are produced from this cluster source. Generated anions enter the extraction region of the TOFMS/PES spectrometer through a 6 mm skimmer. Anions present in the expansion are extracted perpendicularly from the beam by pulsed voltage applied to the first extraction plate. The voltages on the extraction plates are −250 V (pulsed), 0 V, and +750 V, respectively. A liner for both anion and electron flight tube regions has the same voltage (+750 V) as the last extraction plate. Two sets of ion deflector and one ion einzel lens are positioned downstream of the extraction plates. The anions are then analyzed by the oaRETOFMS. Mass resolution, defined as the ability to measure and differentiate between masses, is given by the ratio $m/\Delta m$, in which Δm is the full width at half maximum of the mass feature m of interest. A mass resolution of >1000 is obtained for our mass spectrometer.

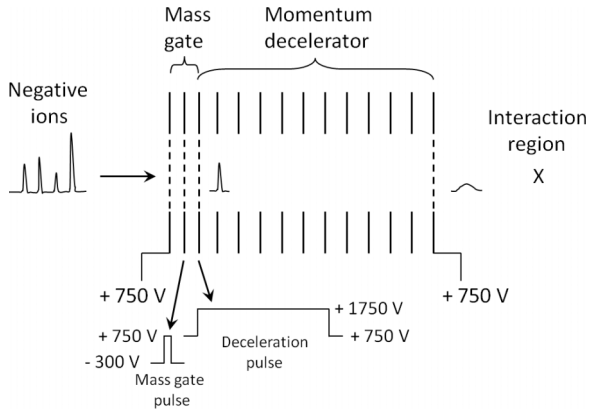

FIG. 3. Details of the mass gate and momentum decelerator portions of the PES apparatus of Figure 1.

The photoelectron technique has the following energy conserving relationship: $h\nu$ = EKE + EBE, in which $h\nu$ is the photon energy, EKE is the measured electron kinetic energy, and EBE is the electron binding energy. In order to obtain a photoelectron spectrum of the anions of interest, a three-grid mass gate is used for cluster and molecule anion mass selection as shown in Figure 3. The first and third grids of the mass gate are at the liner voltage (+750 V), and the middle grid is at negative high voltage −300 V, so that no anions are able to pass. Once the desired anions arrive at the first grid, the high voltage on the middle grid is pulsed to the liner voltage (+750 V) for a short period allowing the anions to pass unaffected. Following the mass gate, the mass selected ion beam enters a momentum decelerator. Once the ion packet passes the third grid of the mass gate, a positive square wave high voltage pulse (+1750 V) is applied to this grid for the momentum deceleration. The subsequent 11 plates of the momentum decelerator are connected by a resistor chain (1 MΩ) in order to create a linearly decreasing deceleration electric field. The last plate of the momentum decelerator is always at the liner voltage (+750 V). The high voltage is pulsed back to the liner voltage before the ion packet leaves the deceleration stack. Both the pulse width and the pulse amplitude can be optimized to achieve the best deceleration effect. This deceleration strategy is broadly used in PES apparatus and has been shown to work quite effectively.[49–52]

The mass selected and decelerated anions are exposed to different laser wavelengths (532 nm, 355 nm, and 266 nm) at the photo-detachment region. A vacuum ultraviolet laser (118 nm, 10.5 eV/photon) and a home-built tabletop extreme ultraviolet (EUV, soft x-ray) laser (26.44 nm, 26.5 eV/photon) are additionally connected to the MBTOF-PES apparatus for high photo-detachment energy PES experiments to expand the detection and characterization ability of the apparatus. The photo-detached electrons are energy analyzed by MBTOF-PES spectrometer. This PES energy analyzer is widely used for the study of clusters due to its high collection efficiency.[51–54] A permanent magnet is used for the high magnetic field (~700 G) generation at the anion beam/photo detachment laser interaction region. The permanent magnet is mounted on a vacuum motor controlled, linear translation stage (Physik Instrumente LPS-24), so that the position of the

permanent magnet can be optimized for the best photoelectron spectrometer resolution. The 1 m electron flight tube is surrounded by a solenoid, which is covered with two layers of GIRON magnetic shielding metal. The electric current for the solenoid is about 0.8 A, which produces a magnetic field of ~10 G at the center of the flight tube. The photo-detached electrons pass through the flight tube and are detected by a microchannel plate (MCP) detector.

Different shape (cylinder, cylinder with a hole at the center, and 75° apex angle cone) magnets are tested to pursue the best photoelectron spectrometer resolution. A 75° apex angle cone shape magnet can improve the resolution of the MBTOF photoelectron spectroscopy compared to the cylindrical magnet. Using the cone shape magnet, a resolution of ~4% (i.e., 40 meV/1.00 eV electron kinetic energy) for the overall MBTOF photoelectron spectroscopy apparatus can be achieved. Under the above operating conditions, PES resolution is no longer limited by Doppler broadening associated with the perpendicular motion of the ion beam with respect to the collection and flight path of the photodetached electrons: in other words, momentum deceleration for the ion cluster beam is efficacious. Improved resolution of the MBTOF spectrometer is also possible, for example, by increasing the length of the electron time of flight tube. PES spectra are collected and calibrated at this resolution with known spectra of Cu^- and Pb^-.[55,56]

When using a 266 nm or higher energy/photon laser as the photo detachment source, background photoelectrons are produced by scattered photons generated by the laser entrance and exit optic windows: these high energy photons strike metal surfaces in the photo-detachment region to generate detected photoelectrons. Different window materials (e.g., CaF_2, sapphire, and fused silica), and different window homogeneity and surface quality, were explored to reduce these background photoelectrons. Of the three potential windows related, background photon scattering sources (materials, homogeneity, and surface quality), the two most important factors are homogeneity and surface quality: window material, as long as the windows do not absorb the laser photons, is not a major source of background scatter. One would anticipate, however, that if high homogeneity and exceptional surface quality could be achieved for window materials, such as LiF and MgF_2, entrance and exit window PES background effects would be further reduced. In the reported experiments, 1-3 angstrom super polished fused silica, Corning grade 0A windows with λ/10 and 10-5 scratch/dig surface quality are used for the least background photoelectrons. As an example of these effects, for Corning grade 0F, λ/8 and 20-10 scratch/dig, standard polished fused silica windows, we find 60/5000 background counts without background subtraction and 20/5000 background counts with alternate laser pulse subtraction. Employing the best fused silica windows described above, these background related counts are both reduced by a factor of 4.

B. Theoretical methods

All calculations are performed using the Gaussian 09 program package.[57] The structures of $FeS_m(SH)_n^-$ (m, n = 0–3, $0 < (m + n) \leq 3$) clusters are optimized for different isomers and spin multiplicities using DFT without constraints. For each cluster, different initial structures are used as input in the optimization procedure. For each structure, spin multiplicities are scanned from low to high until an energy minimum is found. Vibrational frequency calculations are further performed to confirm global minima, which have zero imaginary frequency. The hybrid B3LYP exchange-correlation functional[58–60] with Becke's exchange,[58] and the Perdew and Wang's[61] correlation (BPW91) functional, combined with the triple-ζ valence plus polarization (TZVP) basis set,[62] the 6-311 + G(d) basis set,[63–65] and the large basis set (LBS, aug-cc-PV5Z[66] for sulfur atoms and TZVP for iron and hydrogen atoms), are employed to explore a suitable theoretical level for an accurate description of these iron sulfide, hydrosulfide, and mixed sulfide/hydrosulfide clusters. The choice of these functional and basis sets is based on their good performances for 3*d*-metal oxides/sulfides theoretical studies.[31,46,67] The reliability of the above different computational functionals is evaluated by calculating the first VDE ($VDE = E_{neutral\ at\ optimized\ anion\ geometry} - E_{optimized\ anion}$) of each $FeS_m(SH)_n^-$ (m, n = 0–3, $0 < (m + n) \leq 3$) cluster, which is compared with experimental results. Comparing the first calculated VDEs with their experimentally measured values for $FeS_m(SH)_n^-$ (m, n = 0–3, $0 < (m + n) \leq 3$) clusters at the two different DFT levels, two generalizations can be extracted: 1. calculated properties are insensitive to the basis sets employed, and 2. the BPW91 density functional performs much better than the B3LYP density functional for $FeS_{3-x}(SH)_x^-$ (x = 0-3) cluster anions. For $FeS_{1-x}(SH)_x^-$ (x = 0, 1) (Figure S1(a)) and $FeS_{2-x}(SH)_x^-$ (x = 0-2) (Figure S1(b)) clusters, the B3LYP density functional performs a little better than the BPW91 one (see the supplementary material for details).

Partial charges for the Fe atom of these iron sulfide, hydrosulfide, and mixed sulfide/hydrosulfide clusters are also calculated using both Breneman's CHELPG algorithm[68] and an NBO analysis[69] as implemented in Gaussian 09. CHELPG employs a grid method to select a point at which the electrostatic potential of the molecule is sampled. Fe is assigned a van der Waals radius of 1.95 Å[70] and default atomic radii are used for all other atoms for the CHELPG method.

III. RESULTS AND DISCUSSION

A. Photoelectron spectra of $FeS_m(SH)_n^-$(m, n = 0–3, $0 < (m + n) \leq 3$)

The obtained PES spectra for $FeS_m(SH)_n^-$ (m, n = 0–3, $0 < (m + n) \leq 3$) clusters at different photon energies are shown in Figures 4–6. The first vertical detachment energies (VDEs), proving important in establishing a cluster's electronic and geometric structure, are derived from the energy of the peak maxima in the photoelectron spectra. The first VDEs are the energies of maximum overlap between the nuclear wave functions of the ground states of the anions and their respective neutrals. Our measured first VDEs of FeS_{1-3}^- are 1.85, 3.31, and 2.90 eV, respectively.

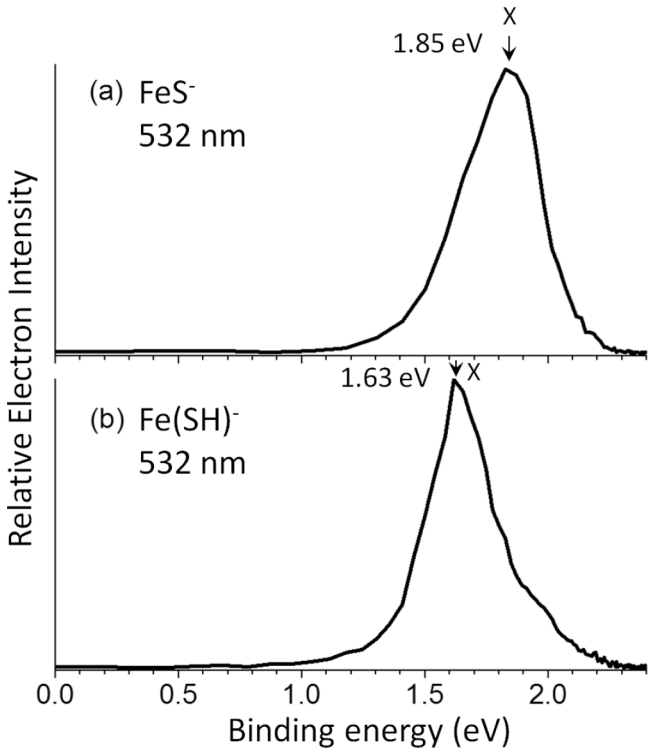

FIG. 4. Photoelectron spectra of (a) FeS^- and (b) $Fe(SH)^-$ at 532 nm. X labels the ground state transition peak.

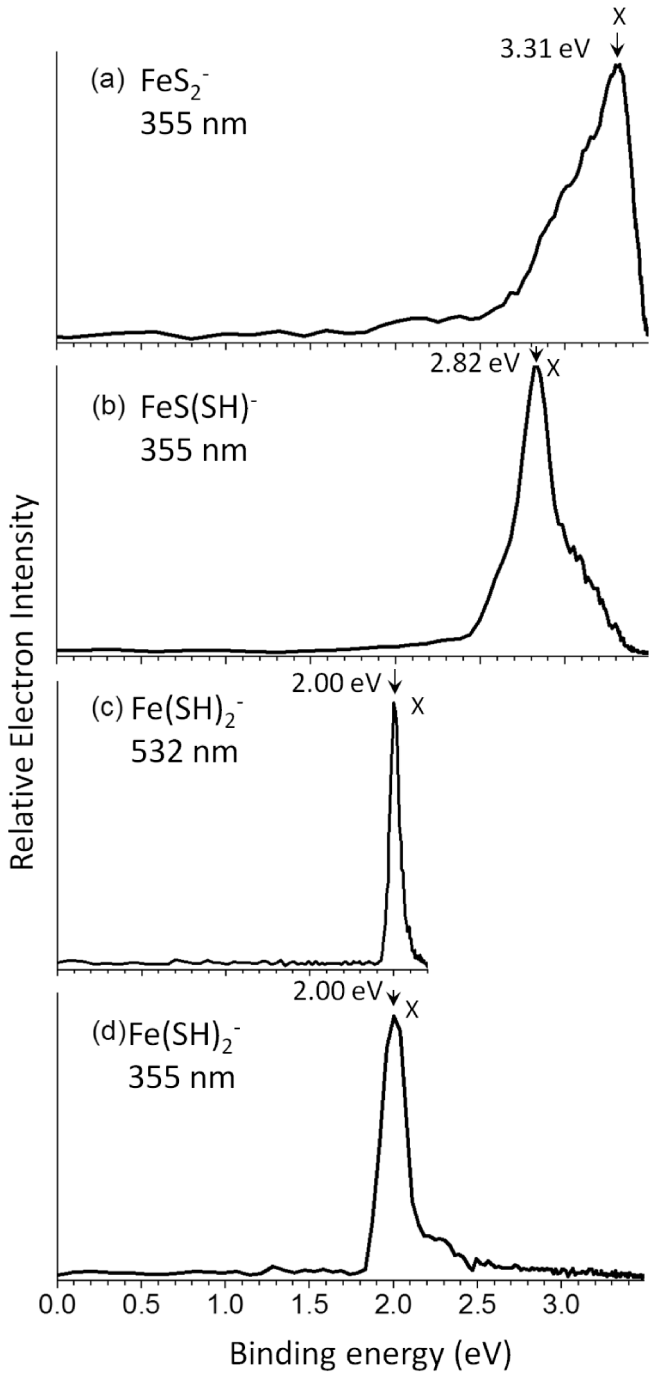

FIG. 5. Photoelectron spectra of (a) FeS_2^- at 355 nm, (b) $FeS(SH)^-$ at 355 nm, (c) $Fe(SH)_2^-$ at 532 nm, and (d) $Fe(SH)_2^-$ at 355 nm. X labels the ground state transition peak.

These results are consistent with the previously reported values of monoiron sulfur clusters.[32] Figure 4(b) shows the photoelectron spectrum for the $Fe(SH)^-$ cluster anion detached by 532 nm (2.331 eV) photons. The first VDE of $Fe(SH)^-$ is 1.63 eV, which is 0.22 eV smaller than that of FeS^-.

Results of the PES experiments for FeS_2^-, $FeS(SH)^-$, and $Fe(SH)_2^-$ clusters are presented in Figure 5. As shown in Figure 5(b), only one primary peak is accessible using 355 nm photon energy, representing the transition from the electronic ground state of $FeS(SH)^-$ to the corresponding neutral electronic ground state. The first VDE for this transition is determined to be 2.82 eV. The PES spectra of $Fe(SH)_2^-$ acquired using photons of 532 nm and 355 nm are displayed in Figures 5(c) and 5(d), respectively. Both results indicate its first VDE is 2.00 eV, the lowest first VDE among those for FeS_2^-, $FeS(SH)^-$, and $Fe(SH)_2^-$ clusters.

Based on the PES spectra of $FeS_{3-x}(SH)_x^-$ (x = 0-3) clusters (Figure 6), the first VDEs of $FeS_2(SH)^-$ (2.80 eV) and $FeS(SH)_2^-$ (2.75 eV) are similar to that of FeS_3^- (2.90 eV), and the first VDE of the hydrosulfide saturated $Fe(SH)_3^-$ is ~0.6 eV smaller than those of the mixed Fe sulfide/hydrosulfide cluster anions.

B. DFT calculations for $FeS_m(SH)_n^-$ and $FeS_m(SH)_n$ (m, n = 0–3, 0 < (m + n) ≤ 3)

Determination of the geometrical structures of the clusters is important, since this cluster property is the basis for the description of all other cluster characteristics (e.g., electronic structure, electron density, charge and spin densities, etc.). Here, structures for various states of different spin multiplicities are investigated for each cluster. The energy differences (ΔE) between low lying states of different spin multiplicity states of each cluster are calculated and compared to evaluate their relative stabilities. Structures of the two lowest lying states of different spin multiplicities of each cluster are presented and the first VDE for each state (isomer) is calculated. The spin multiplicity for the ground state of a cluster anion $FeS_m(SH)_n^-$ (m, n = 0–3, 0 < (m + n) ≤ 3) is assigned mainly based on agreement of the first calculated

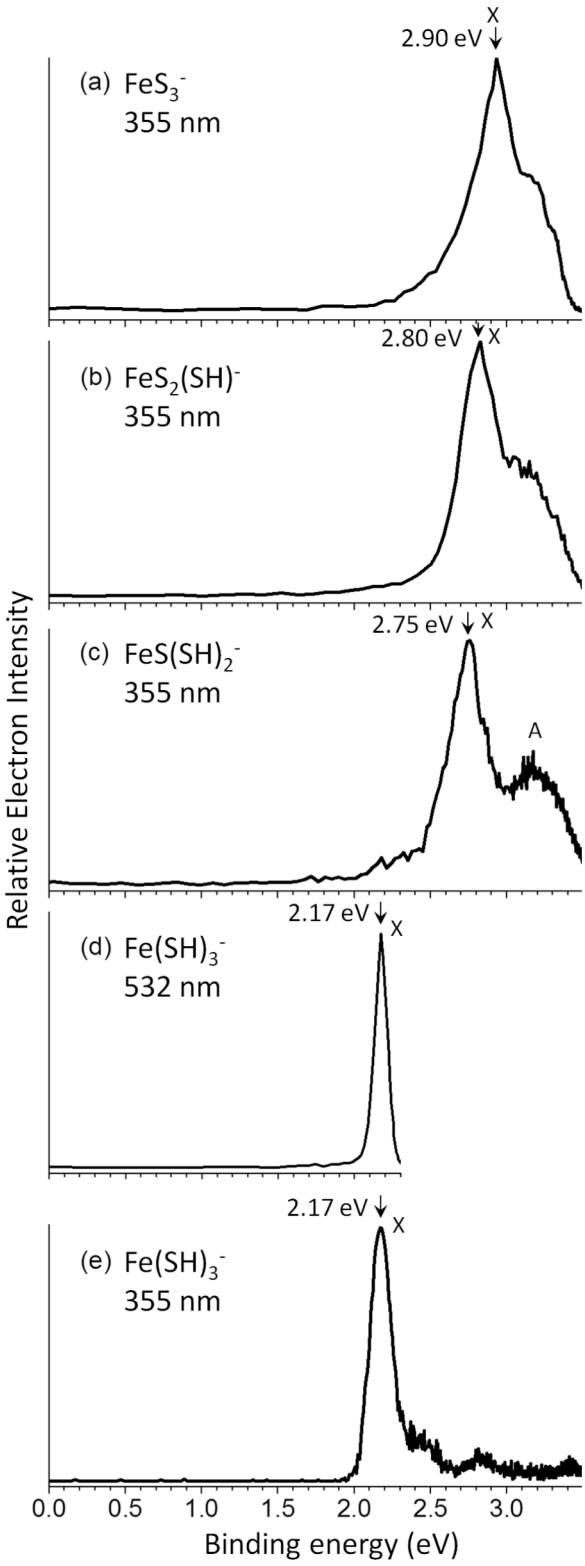

FIG. 6. Photoelectron spectra of (a) FeS_3^- at 355 nm, (b) $FeS_2(SH)^-$ at 355 nm, (c) $FeS(SH)_2^-$ at 355 nm, (d) $Fe(SH)_3^-$ at 532 nm, and (e) $Fe(SH)_3^-$ at 355 nm. X labels the ground state transition peak and A labels the low-lying transition peak next to X.

VDEs for the different spin multiplicities compared to the experimental values. The ΔE between the two spin states under consideration is also evaluated and employed to generate the assignment. Figures 7 and 8 present the optimized geometries

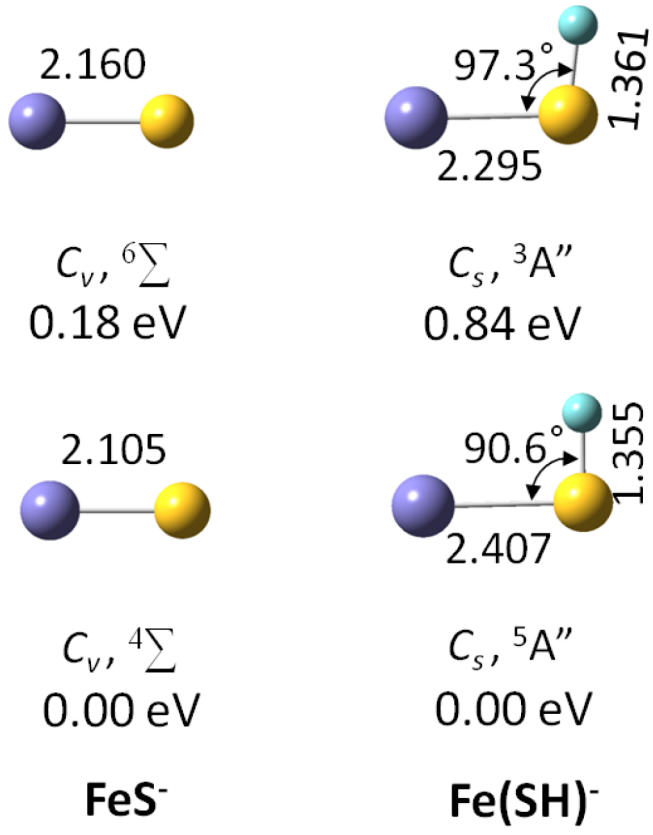

FIG. 7. DFT optimized structures of FeS^- and $Fe(SH)^-$ at the B3LYP/TZVP level. Relative energies are corrected for ZPE and are given in eV underneath each structure. For each structure, bond lengths (in angstroms), important bond angel, point group symmetry, and electronic state are listed.

of $FeS_{1-x}(SH)_x^-$ (x = 0, 1) and $FeS_{2-x}(SH)_x^-$ (x = 0-2) clusters at the B3LYP/TZVP level of theory, respectively. Geometries displayed in Figures 7 and 8 will be the focus of the following discussions. The optimized geometries for $FeS_{3-x}(SH)_x^-$ (x = 0-3) cluster anions are, on the other hand, displayed at both the B3LYP/TZVP and BPW91/TZVP levels of theory in Figure 9. In Figures 7–9, bond lengths, bond angles, spin multiplicities, and ΔEs between different spin states of these clusters are presented. The first calculated VDEs and ΔEs of these clusters obtained at different theoretical levels are also summarized in Tables I–III. ΔEs are corrected for zero point energies. ΔE = 0.00 eV means that the energy of the given spin multiplicity structure is the lowest one among all possible spin multiplicity structures.

The spin multiplicities of ground state FeS^- and $Fe(SH)^-$ clusters (Figure 7) are quartet and quintet, respectively. The theoretically determined quartet spin multiplicity of ground state FeS^- agrees with the result reported in other theoretical studies.[40] The Fe–S bond lengths of ground state FeS^- and $Fe(SH)^-$ clusters are calculated to be 2.105 and 2.407 Å, respectively. An approximate 0.3 Å elongation of the Fe–S bond length occurs for $Fe(SH)^-$ with respect to the bond length for FeS^-. Figure 8 depicts geometries of $FeS_{2-x}(SH)_x^-$ (x = 0-2) clusters. The zero point energy of sextet FeS_2^- is lower than that of quartet FeS_2^- by 0.21 eV at the B3LYP/TZVP level (Table II), and the theoretical first VDE of sextet FeS_2^- is closer to the experimental value than that of quartet FeS_2^-.

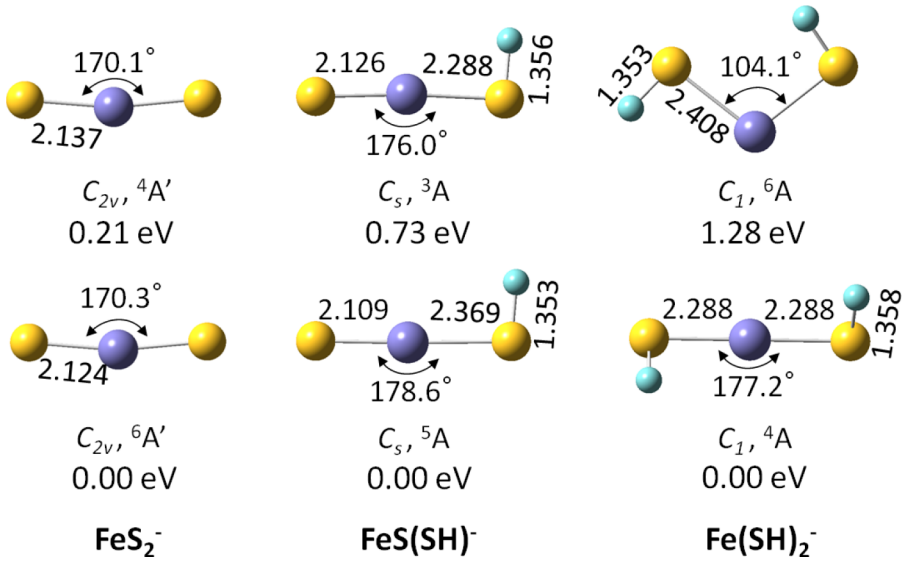

FIG. 8. DFT optimized structures of $FeS_{2-x}(SH)_x^-$ (x = 0-2) at the B3LYP/TZVP level. Relative energies are corrected for ZPE and are given in eV underneath each structure. For each structure, bond lengths (in angstroms), important bond angel, point group symmetry, and electronic state are listed.

Thus, the spin multiplicity of ground state FeS_2^- is assigned to be sextet. In like manner, quintet $FeS(SH)^-$ and quartet $Fe(SH)_2^-$ are found to be their respective lowest energy spin multiplicities. The first calculated VDE for quintet $FeS(SH)^-$ is 2.73 eV, obviously closer to its respective experimental value (2.82 eV) than that for the triplet $FeS(SH)^-$ (2.04 eV): quintet $FeS(SH)^-$ (structure shown in Figure 8) is, thereby, suggested to be its ground state. The observed first VDE for $Fe(SH)_2^-$ is 2.00 eV; the first calculated VDE for quartet and sextet $Fe(SH)_2^-$ are 1.88 eV and 1.41 eV at B3LYP/TZVP level, respectively. Therefore quartet $Fe(SH)_2^-$, which has a linear S–Fe–S structure, is assigned as the ground state of $Fe(SH)_2^-$. As presented in Figure 8, the Fe–S bond length of ground state FeS_2^- cluster is 2.124 Å. The Fe–(SH) bond length of ground state $Fe(SH)_2^-$ cluster is 2.288 Å. The Fe–S bond length of ground state $FeS(SH)^-$ cluster is 2.109 Å, which is shorter than that of FeS_2^- (2.124 Å): the Fe–(SH) bond length for these two sulfur atoms containing cluster is calculated to be 2.369 Å, longer than that of $Fe(SH)_2^-$ (2.288 Å). The Fe–(SH) bond length is roughly 0.2 Å longer than the Fe–S bond length in $FeS_{2-x}(SH)_x^-$ (x = 0-2) clusters.

Theoretical study of $FeS_{3-x}(SH)_x^-$ (x = 0-3) cluster anions becomes a little more complicated due to more sulfur atoms and (SH) groups, so different density functionals and basis sets (summarized in Table III) are required to yield accurate calculational results for this Fe/S/SH, three S atom cluster series. If different basis sets combined with the specific density functional BPW91 are employed in these calculations, the obtained ΔEs and first VDEs for each $FeS_{3-x}(SH)_x^-$ (x = 0-3) cluster anion are different by <0.3 eV. For example, using the BPW91 density functional combined with 6-311 + G(d), TZVP, and LBS basis sets, the first calculated VDEs for the triplet state of $Fe(SH)_3^-$ are 2.49 eV, 2.23 eV, and 2.42 eV. The calculated ΔEs for this cluster are 0.68 eV, 0.80 eV, and 0.67 eV, respectively. The first calculated VDE difference in this comparison is ≤0.23 eV. The calculated ΔE difference in this comparison is ≤0.13 eV. This performance suggests that the calculated properties of $FeS_{3-x}(SH)_x^-$ (x = 0-3) clusters are insensitive to the employed basis sets: the different performances of B3LYP and BPW91 density functionals are thus only compared through results of the TZVP basis set (see details in the supplementary material). The calculated results of $FeS_{3-x}(SH)_x^-$ (x = 0-3) clusters at the BPW91/TZVP level will be the focus of the following discussions.

The first calculated VDE of sextet FeS_3^- employing the BPW91 density functional is only about 0.16 eV closer to the respective experimental value than that of the quartet FeS_3^- (Table III). The ΔE between the quartet and sextet FeS_3^- clusters is also very small (<0.05 eV). These results suggest that the spin multiplicity of ground state FeS_3^- is more likely sextet, but quartet FeS_3^- clusters can also exist in the experimental sample. Additionally, given the spin orbit coupling for a metal like Fe, one can expect some degree of sextet/quartet spin mixing for a final, more exact description for the ground state of FeS_3^-. The optimized structures of the sextet FeS_3^- displayed in Figure 9 demonstrate that an S–S bond is formed in this cluster, with a bond length of ~2.19 Å. Two types of Fe–S bonds are thereby characterized for FeS_3^-: an Fe–S bond, at ~2.10 Å, and an Fe–(S_2) symmetrical bond at ~2.28 Å. Formation of the S–S bond decreases the Fe/S bonding interaction, as the length of the Fe–(S_2) bond is longer than that of the Fe–S bond. Triplet and quintet are the two lowest energy spin multiplets of $FeS_2(SH)^-$. The zero point energy of quintet $FeS_2(SH)^-$ is 0.12 eV higher than that of triplet $FeS_2(SH)^-$. Structures for the most stable spin state of $FeS_2(SH)^-$ are displayed in Figure 9 at the different theoretical levels. An S–S bond is not evident in the structure of triplet $FeS_2(SH)^-$ obtained at BPW91/TZVP level. The first calculated VDE of triplet $FeS_2(SH)^-$ (2.72 eV) employing BPW91 functional is in good agreement with the respective experimental measurement (2.80 eV). The spin multiplicities of ground state $FeS(SH)_2^-$ and $Fe(SH)_3^-$ clusters are assigned to be sextet and quintet, respectively. An S–S bond is not observed in their structures (Figure 9). The bond length of an Fe–S bond is about 2.1 Å, and that of Fe–(SH) bond is about 2.3 Å. The first calculated VDEs of

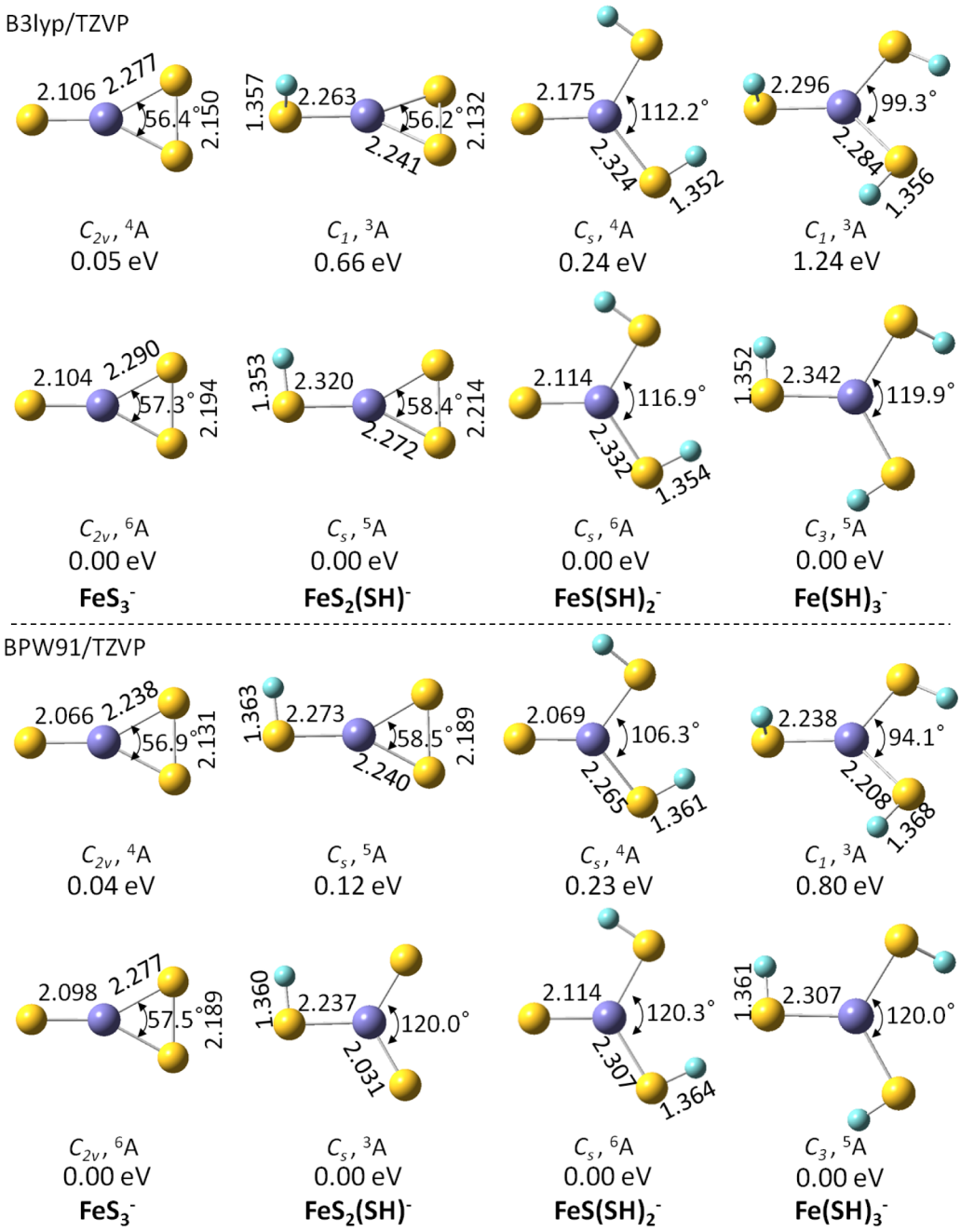

FIG. 9. DFT optimized structures of $FeS_{3-x}(SH)_x^-$ (x = 0-3)at B3LYP/TZVP and BPW91/TZVP levels. Relative energies are corrected for ZPE and are given in eV underneath each structure. For each structure, bond lengths (in angstroms), important bond angel, point group symmetry, and electronic state are listed.

ground state $FeS(SH)_2^-$ and $Fe(SH)_3^-$, employing the BPW91 density functional, are in agreement with their experimental values.

Adiabatic electron affinity ($EA = E_{optimized\ neutral} - E_{optimized\ anion}$) for each ground state $FeS_m(SH)_n$ (m, n = 0–3, $0 < (m + n) \leq 3$) neutral cluster, assigned through the above results, is calculated and summarized in Table IV. Neutral cluster experimental EAs are also listed for comparison. EAs of $FeS_{1-x}(SH)_x$ (x = 0, 1) and $FeS_{2-x}(SH)_x$ (x = 0-2) clusters are calculated at B3LYP/TZVP level, and EAs of $FeS_{3-x}(SH)_x$ (x = 0-3) clusters are calculated at BPW91/TZVP level. Note that the obtained experimental EAs of iron sulfide and mixed sulfide/hydrosulfide clusters are possibly more affected by their anion vibrational hot bands than are the EAs for pure $Fe(SH)_n$ clusters due to their higher temperature generation conditions (~3.5 mJ/pulse ablation laser energy). Thus, experimental EAs for iron sulfide FeS_m and mixed sulfide/hydrosulfide $FeS_m(SH)_n$ clusters are possibly more underestimated in this work than are the EAs for iron hydrosulfide $Fe(SH)_n$ pure neutral clusters.

C. Comparison of FeS_m^- and $Fe(SH)_n^-$ (m, n = 1–3) cluster anions

The (SH) group plays an important role in activating enzymes and proteins, for which iron sulfur clusters are the

TABLE I. The first calculated VDEs (in eV) of FeS^- and $Fe(SH)^-$ at B3LYP/TZVP and BPW91/TZVP levels, as well as the experimental results for comparison. Calculated relative energy differences for the two indicated low lying spin states ΔE (in eV, not VDE difference) are given in parenthesis. $\Delta E = 0.00$ eV means the energy of that spin multiplicity structure is the lowest one among all possible spin multiplicity structures.

		VDE (eV)		
Cluster	Spin multiplicity	B3LYP/TZVP (ΔE)	BPW91/TZVP (ΔE)	Experimental
FeS^-	6	1.32 (0.18)	1.05 (0.17)	1.85 [8][a]
	4	1.43 (0.00)	1.12 (0.00)	
$Fe(SH)^-$	3	0.50 (0.84)	0.34 (0.69)	1.63 [8]
	5	1.48 (0.00)	1.13 (0.00)	

[a]The numbers in square brackets indicate the uncertainties in the last digit.

TABLE II. The first calculated VDEs (in eV) of $FeS_{2-x}(SH)_x^-$ ($x = 0$-2) at the B3LYP/TZVP and BPW91/TZVP levels, as well as the experimental results for comparison. Calculated relative energy differences for the two indicated low lying spin states ΔE (in eV, not VDE difference) are given in parenthesis.

		VDE (eV)		
Cluster	Spin multiplicity	B3LYP/TZVP (ΔE)	BPW91/TZVP (ΔE)	Experimental
FeS_2^-	4	3.22 (0.21)	2.80 (0.15)	3.31 [8][a]
	6	3.40 (0.00)	3.12 (0.00)	
$FeS(SH)^-$	3	2.04 (0.73)	2.05 (0.64)	2.82 [8]
	5	2.73 (0.00)	2.48 (0.00)	
$Fe(SH)_2^-$	6	1.41 (1.28)	1.17 (1.37)	2.00 [8]
	4	1.88 (0.00)	1.78 (0.00)	

[a]The numbers in square brackets indicate the uncertainties in the last digit.

putative active centers. As we have emphasized above, the number of (SH) groups and S atoms in a nonmixed cluster has a significant electronic and structural effect on the general properties of iron sulfide and iron hydrosulfide clusters. A good way to explore these effects is comparing the property of (SH) group saturated iron hydrosulfide clusters with those of pure iron sulfide clusters. Figure 10 plots the trends of experimental first VDEs as a function of n for $Fe(SH)_n^-$ and of m for FeS_m^-. The first VDE for Fe^- is taken from Refs. 71 and 72. The experimental first VDEs for $Fe(SH)_n^-$ are consistently smaller than those of FeS_m^- ($n = m$ = 1-3). Experimental first VDEs of $Fe(SH)_{0-3}^-$ clusters are observed to increase with added (SH) groups, for which each (SH) group is responsible for an increase in the first VDE of ~1.5, ~0.4, and ~0.2 eV, respectively. The experimental first VDEs for FeS_{0-3}^- clusters are observed, however, to increase for the first two added S atoms, but to decrease for the third S atom. Each of the first two S atoms is responsible for a large increase of the first VDE, ~1.7 and ~1.5 eV, respectively, whereas the third S atom is responsible for a decrease in the first VDE of ~0.4 eV.

Electron affinity (EA) is a measure of the minimum amount of energy required to remove an electron from the anion in its ground state. For these iron sulfide and iron hydrosulfide cluster anions, because both the S atom and the (SH) group are much more electronegative than the central iron atom, electron density should be removed from the iron atom of these clusters. Naturally, partial atomic charges play a decisive role in determining the core electron binding energy in small molecules.[73] The partial charge of the iron atom in these iron sulfide and iron hydrosulfide cluster anions can to some extent affect the energy required to remove an electron from such clusters. To investigate the dependence of the partial charge of the Fe atom on the number of S atoms and (SH) groups, calculated partial charges for Fe atoms of ground state FeS_m^- (m = 1–3) and $Fe(SH)_n^-$ (n = 1–3) clusters, using both the CHELPG and NBO analyses at the BPW91/TZVP level, are plotted in Figure 11 as a function of cluster size (n and m). The partial charge number for Fe atoms of these clusters obtained by either a CHELPG or NBO analysis is slightly different, but their trends with cluster size are in good agreement with each other. Calculated partial charges for the Fe atom of ground state FeS_{0-3}^- clusters are found to increase for the first two S atoms added to Fe. Atomic sulfur is a highly electronegative atom and thus more S atoms binding with the central Fe atom generate a more positive Fe atom: that is,

TABLE III. The first calculated VDEs (in eV) for $FeS_{3-x}(SH)_x^-$ ($x = 0$-3) using different functionals and basis sets, as well as the experimental results for comparison, are the main entries in the table. Large basis set (LBS) denotes an aug-cc-PV5Z basis set for all sulfur atoms and a TZVP basis set for iron and hydrogen atoms. Calculated relative energy differences for the two indicated low lying spin states ΔE (in eV, not VDE difference) are given in parenthesis.

		VDE (eV)						
		B3LYP			BPW91			
Cluster	Spin multiplicity	6-311 + G(d) (ΔE)	TZVP (ΔE)	LBS (ΔE)	6-311 + G(d) (ΔE)	TZVP (ΔE)	LBS (ΔE)	Exp.
FeS_3^-	4	3.11 (0.01)	2.93 (0.05)	3.01 (0.00)	2.66 (0.00)	2.47 (0.04)	2.57 (0.00)	2.90 [8][a]
	6	3.18 (0.00)	3.04 (0.00)	3.06 (0.00)	2.76 (0.00)	2.63 (0.00)	2.64 (0.03)	
$FeS_2(SH)^-$	3	2.48 (0.66)	2.29 (0.66)	2.37 (0.62)	2.88 (0.00)	2.72 (0.00)	2.83 (0.00)	2.80 [8]
	5	2.91 (0.00)	2.78 (0.00)	2.78 (0.00)	2.49 (0.19)	2.35 (0.12)	2.40 (0.03)	
$FeS(SH)_2^-$	4	3.37 (0.24)	3.27 (0.24)	3.30 (0.24)	2.83 (0.16)	2.69 (0.23)	2.74 (0.18)	2.75 [8]
	6	3.64 (0.00)	3.50 (0.00)	3.57 (0.00)	3.13 (0.00)	3.00 (0.00)	3.07 (0.00)	
$Fe(SH)_3^-$	3	2.72 (1.12)	2.50 (1.24)	2.62 (1.20)	2.49 (0.68)	2.23 (0.80)	2.42 (0.67)	2.17 [8]
	5	3.49 (0.00)	3.35 (0.00)	3.40 (0.00)	2.87 (0.00)	2.64 (0.00)	2.74 (0.00)	

[a]The numbers in square brackets indicate the uncertainties in the last digit.

TABLE IV. Calculated adiabatic electron affinity (EA) of ground state $FeS_m(SH)_n$ (m, $n = 0$–3, $0 < (m+n) \leq 3$) clusters, as well as their experimental EAs for comparison. EAs of $FeS_{1-x}(SH)_x$ ($x = 0$, 1) and $FeS_{2-x}(SH)_x$ ($x = 0$-2) clusters are calculated at the B3LYP/TZVP level, and EAs of $FeS_{3-x}(SH)_x$ ($x = 0$-3) clusters are calculated at the BPW91/TZVP level. Spin multiplicity (M) is listed as $^M FeS_m(SH)_n$.

Cluster	Calculated EA	Experimental EA
^5FeS	1.39	1.60 [10][a]
$^4Fe(SH)$	1.31	1.40 [10]
$^7FeS_2$	3.36	3.10 [10]
$^6FeS(SH)$	2.65	2.60 [10]
$^5Fe(SH)_2$	1.86	1.94 [10]
$^5FeS_3$	2.50	2.70 [10]
$^4FeS_2$ (SH)	2.71	2.60 [10]
$^5FeS(SH)_2$	2.83	2.50 [10]
$^6Fe(SH)_3$	2.54	2.05 [10]

[a]The numbers in square brackets indicate the uncertainties in the last digit.

the positive partial charge on the central Fe atom of these FeS_{0-3}^- cluster anions should increase. Based on the trend for the first two S atoms as presented in Figure 11, the partial charge for the Fe atom is anticipated to increase to around 1.4 for the FeS_3^- cluster. Nonetheless, partial charge for the Fe atom of FeS_3^-, obtained both by CHELPG and NBO analyses, decreases ~0.1 compared with that of the FeS_2^- cluster. This observation is in good agreement with the trend in experimental first VDEs of FeS_{0-3}^- clusters as a function of S atom number (as shown in Figure 10). These results are understandable because of the formation of an S–S bond in the FeS_3^- cluster. Length of the Fe–(S_2) bond (2.290 Å) for FeS_3^- is 0.166 Å longer than that of the Fe–S bond (2.124 Å) for FeS_2^-, as calculated at the B3LYP/TZVP level and shown in Figures 8 and 9. The interaction between Fe and the S–S unit in FeS_3^- is weaker than that between Fe and S in FeS_2^-: the Fe atom in FeS_3^- donates less electron density to the S–S unit than does the Fe atom in FeS_2^- and therefore

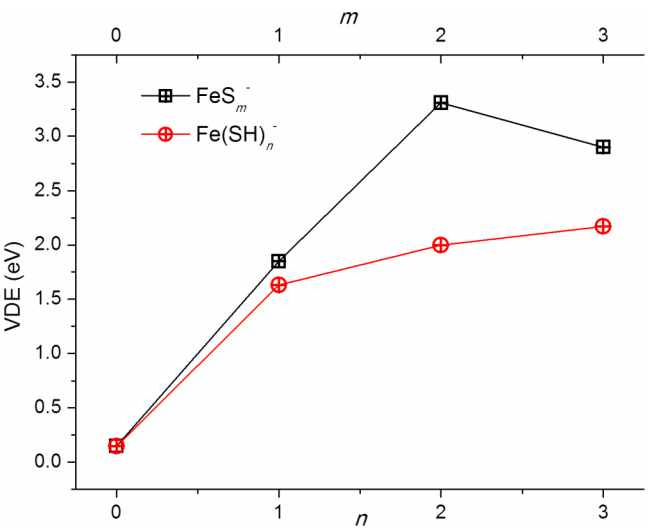

FIG. 10. Observed electron binding energies (the first VDEs) of FeS_m^- ($m = 0$–3) and $Fe(SH)_n^-$ ($n = 0$–3) as a function of number m and n. The first VDE for Fe^- is taken from Refs. 71 and 72.

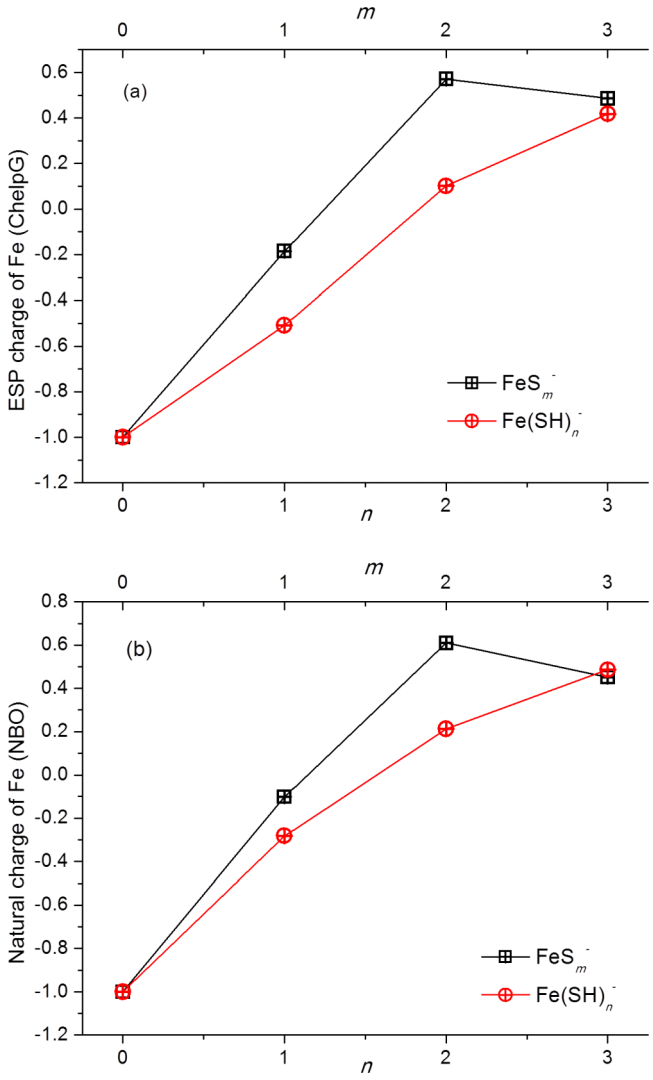

FIG. 11. Calculated partial charge of the Fe atom of ground state FeS_m^- ($m = 0$–3) and $Fe(SH)_n^-$ ($n = 0$–3) clusters employing (a) the CHELPG method and (b) NBO analysis at the BPW91/TZVP level as a function of number m and n.

has a lower positive partial charge number. The above results and analyses are helpful and reasonable for understanding and explaining the observed decrease of experimental first VDE for FeS_3^- compared to that for FeS_2^- as presented in Figure 10.

No S–S interactions are evident for ground state $Fe(SH)_{0-3}^-$ clusters, and thus calculated partial charges for the Fe atom of these clusters are found to increase approximately linearly with the number of (SH) groups present. Observation of smaller partial charges for the Fe atoms of $Fe(SH)_n^-$ than for those of FeS_m^- (Figure 11) agrees well with the smaller experimental first VDEs for $Fe(SH)_n^-$ than for FeS_m^- ($n = m > 0$) (Figure 10). The Pauling electronegativity of the Fe atom is 1.83, the H atom is 2.20, the S atom is 2.58, and the (SH) group is 2.44 (calculated according to the group electronegativity equation[74,75]). Electronegativity of the (SH) group is obviously smaller than that of the S atom, so (SH) group bonding to the Fe atom of a cluster generates a smaller positive partial charge for the Fe atom than does the same number of bonded S atoms. This relationship between

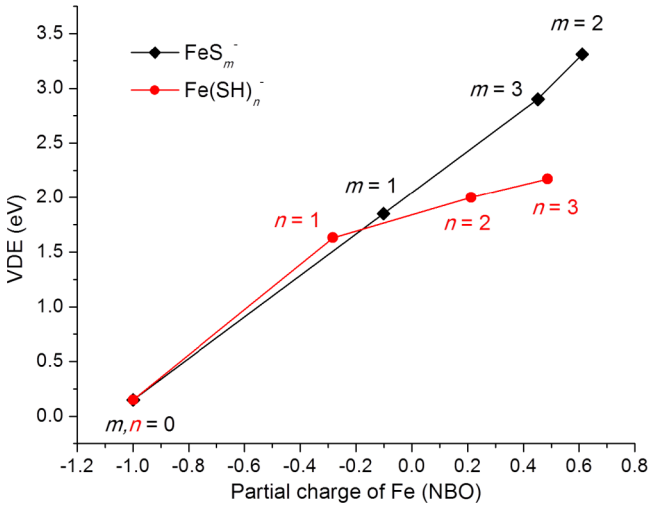

FIG. 12. The observed first VDEs of FeS_m^- ($m = 0$–3) and $Fe(SH)_n^-$ ($n = 0$–3) as a function of calculated partial charge of the Fe atom employing the NBO analysis at BPW91/TZVP level. Results for the B3LYP/TZVP calculation are very similar.

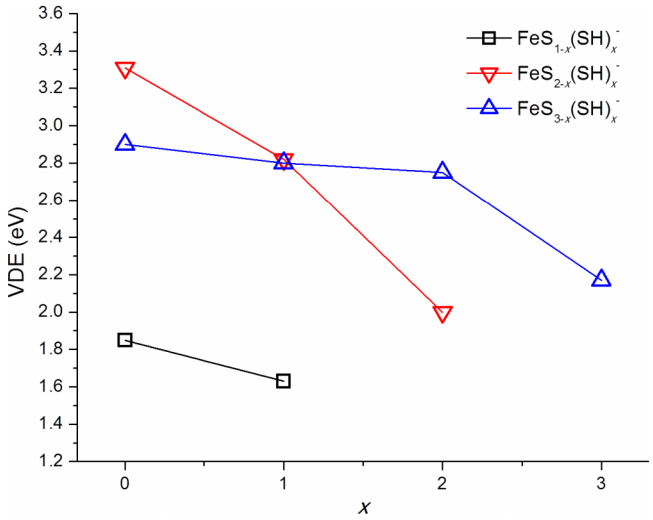

FIG. 13. The observed first VDEs of $FeS_{1-x}(SH)_x^-$ ($x = 0$, 1), $FeS_{2-x}(SH)_x^-$ ($x = 0$-2), and $FeS_{3-x}(SH)_x^-$ ($x = 0$-3) as a function of (SH) group number x.

partial atomic charge for Fe and ligand electronegativity can rationalize the observed trend of smaller first VDEs for $Fe(SH)_n^-$ than for FeS_m^- ($n = m > 0$) cluster anions.

A better understanding of the relationship between partial atomic charge for the Fe atom of ground state FeS_{0-3}^- and $Fe(SH)_{0-3}^-$ clusters and their experimental first VDEs emerges from a plot of the first VDEs as a function of calculated partial charge of Fe atoms, as presented in Figure 12. The first cluster VDEs clearly increase with partial charge of the Fe atom; in other words, a higher first VDE is correlated with a higher, more positive partial charge for the Fe atom of these clusters. The different slope of the trend of the first VDE of FeS_{0-3}^- and $Fe(SH)_{0-3}^-$ clusters with their partial charge for the Fe atom (m, n = 1, 2, 3) is probably due to the intrinsic bonding/electronic structure property of the S atom and (SH) group.

Above results and discussion suggest that the change of partial charge for the Fe atom of ground state FeS_{0-3}^- and $Fe(SH)_{0-3}^-$ clusters as a function of different S atom and (SH) group number is possibly responsible for their experimental first VDE trends. For a qualitative understanding and estimation of the change of first VDEs of ground state iron sulfide and iron hydrosulfide cluster anions with respect to the number of cluster S atoms and (SH) groups, partial charge of the Fe atom is a good reference value: a higher, more positive partial charge for the cluster Fe atom is indicative of a higher cluster first VDE.

D. Comparison of various iron sulfide/hydrosulfide mixed cluster anions

Sulfur atoms and (SH) groups in reactive iron sulfide/hydrosulfide sites usually coexist in real biochemical and catalytic systems; thus, exploring their relative behavior in mixed clusters with different (SH) group content may provide useful information for understanding the chemistry and mechanisms of these species in real, complex systems. Figure 13 plots the trend of experimental first VDEs of $FeS_{1-x}(SH)_x^-$ (x = 0, 1), $FeS_{2-x}(SH)_x^-$ (x = 0-2), and $FeS_{3-x}(SH)_x^-$ (x = 0-3) clusters as a function of (SH) group number x. As discussed in Section III C, the experimental first VDE for $FeSH^-$ is smaller than that for FeS^-. Looking at the red line (∇) shown in the figure, the experimental first VDE for $FeS(SH)^-$ is observed ~0.49 eV lower than that for FeS_2^- and ~0.82 eV higher than that for $Fe(SH)_2^-$. The experimental first VDEs for $FeS_2(SH)^-$ and $FeS(SH)_2^-$ clusters are observed to behave similarly (within ~0.15 eV) with respect to FeS_3^-; however, ~0.6 eV higher than that for the (SH) group saturated $Fe(SH)_3^-$ cluster, as plotted by the blue line (Δ) in Figure 13.

To investigate how calculated partial charges for the Fe atom of these iron sulfide/hydrosulfide mixed clusters are related to their experimental first VDEs, calculated partial charges for cluster Fe atoms using CHELPG and NBO analyses (employing BPW91/TZVP) as a function of (SH) group number are presented in Figure 14. Results for their respective iron sulfide and iron hydrosulfide nonmixed clusters are also presented in the figure for comparison. The calculated partial charge on the Fe atom of ground state $FeS(SH)^-$ is lower than that of FeS_2^- and higher than that of $Fe(SH)_2^-$, which is in agreement with their experimental first VDE trends as a function of (SH) group number x. The calculated partial charges for the Fe atoms of FeS_2^-, $FeS(SH)^-$, and $Fe(SH)_2^-$ decrease with the increase of (SH) group content because the electronegativity of the (SH) group is smaller than that of a single S atom. This suggests an increase of (SH) ligands in the cluster generates a lower cluster first VDE.

On the other hand, no obvious similar trend for Fe partial charge vs. the first VDE is found for results of $FeS_2(SH)^-$ and $FeS(SH)_2^-$ clusters compared to those of FeS_3^- and $Fe(SH)_3^-$. The existing S–S bond in the cluster, as discussed in Section III C, lowers the experimental first VDE for FeS_3^-. The disulfide S–S bond is not observed for ground state $FeS_2(SH)^-$ and $FeS(SH)_2^-$ clusters (as shown in Figure 9); nonetheless, these latter mixed clusters contain more (SH) groups than

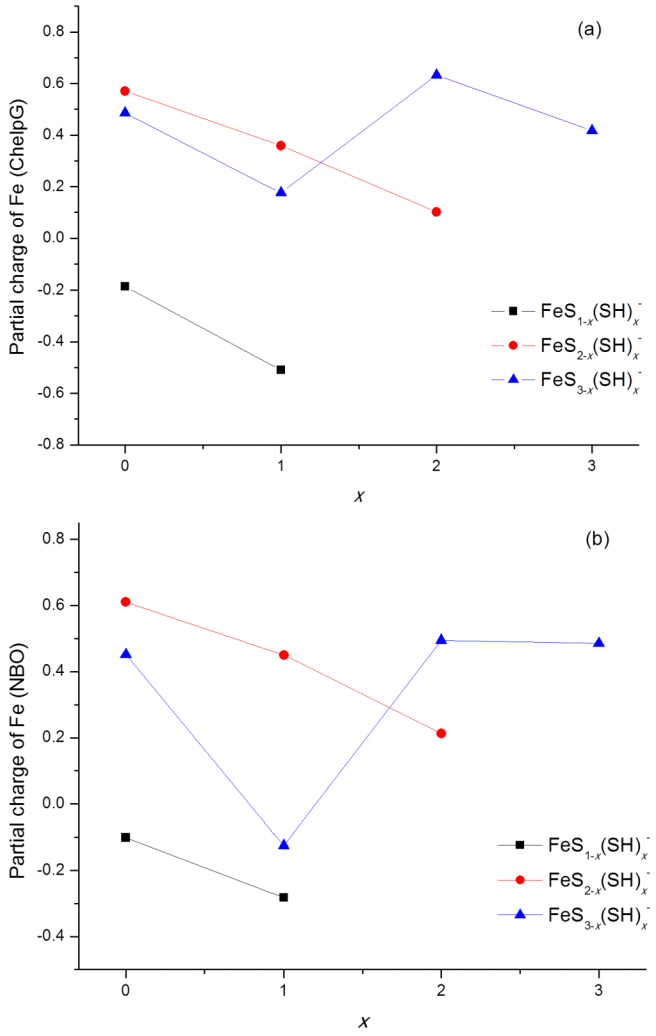

FIG. 14. Calculated partial charge of the Fe atom of ground state $FeS_{1-x}(SH)_x^-$ ($x = 0$, 1), $FeS_{2-x}(SH)_x^-$ ($x = 0$-2), and $FeS_{3-x}(SH)_x^-$ ($x = 0$-3) clusters employing (a) the CHELPG method and (b) NBO analysis at the BPW91/TZVP level as a function of (SH) group number x.

FeS_3^-, which lowers their first VDEs. These two factors, S–S bonding and S/(SH) electronegativity differences, may well be responsible for the similar first VDEs for $FeS_2(SH)^-$, $FeS(SH)_2^-$, and FeS_3^- clusters (see Figure 13). Unexpectedly, an "out-of-order" partial charge of the Fe atom of these clusters is observed (Figure 14). Other possible factors may affect or relate to the experimental first VDEs of these iron sulfide/hydrosulfide mixed cluster anions, but, as shown in Figure S2 in the supplementary material, no obvious similar electronic or structure trends that parallel the first VDEs results and trends (Figure 13) are observed for $FeS_2(SH)^-$, $FeS(SH)_2^-$, and FeS_3^- clusters by considering either: 1. calculated partial charges for the Fe atom of ground state neutral clusters, 2. spin density for the Fe atom of either the ground state anion and neutral clusters, or 3. details of the specific orbital patterns for anionic or neutral clusters in this series at the DFT/basis set levels considered herein.

The above results suggest that more (SH) group content in iron sulfide/hydrosulfide mixed clusters is correlated with a lower first VDE and a lower partial charge of the Fe atom for the cluster anion (see Figure 13). The calculated partial charge of the Fe atom of such clusters is, therefore, a useful reference factor for a qualitative understanding of the change of first VDEs as the S/(SH) content of the cluster changes. Nonetheless, the trend in the first VDEs for these clusters is clearly not simply related to the Fe partial charge (see Figures 13 and 14 for $FeS_{3-x}(SH)_x$, blue line (Δ): for a more quantitative understanding of the relative first VDEs of these S/(SH) Fe clusters one must consider higher level treatments of their electronic structure, such as CASSCF and CASPT2 methods.

IV. CONCLUSIONS

A magnetic-bottle time-of-flight photoelectron spectroscopy (MBTOF-PES) apparatus is constructed in our lab. A mass resolution ($M/\Delta M$) of more than 1000 is obtained by the coupled orthogonal acceleration/extraction reflectron time of flight mass spectrometer (oaRETOFMS). The MBTOF-PES apparatus has a measured resolution of ~40 meV for an electron of ~1.0 eV kinetic energy. The PES spectra of small iron sulfide, hydrosulfide, and mixed sulfide/hydrosulfide [$FeS_m(SH)_n^-$; (m, n = 0–3, 0 < (m + n) ≤ 3)] cluster anions, at 2.331 eV (532 nm) and 3.492 eV (355 nm) photon energies, are reported. The structural and bonding properties of these clusters are investigated at different levels of Density Functional Theory (DFT) and basis sets. The calculated cluster properties are insensitive to the basis set employed; nonetheless, the density functional BPW91 performs better for a theoretical description of these clusters, and is thereby employed and recommended, along with the TZVP basis set, for an accurate theoretical depiction of the iron sulfide, hydrosulfide, and mixed sulfide/hydrosulfide clusters under consideration. The most probable structures, electronic properties, and ground state spin multiplicities for $FeS_m(SH)_n^-$ (m, n = 0–3, 0 < (m + n) ≤ 3) clusters are tentatively assigned by comparing their theoretical and experimental first vertical detachment energy (VDE) values. Calculated and experimental adiabatic electron affinities of these ground state $FeS_m(SH)_n$ (m, n = 0–3, 0 < (m + n) ≤ 3) clusters are also reported. A comparison of S and (SH) as ligands in these iron sulfide and hydrosulfide cluster anions is investigated. The combined theoretical and experimental results can be summarized as follows: 1. lower respective experimental first VDEs for $Fe(SH)_n^-$ than for FeS_m^- ($n = m$ = 1–3) are observed; 2. the experimental first VDEs for FeS_m^- (m = 1–3) cluster anions are observed to increase with the addition of the first two S atoms to the Fe atomic center, but to decrease for the third added S atom; 3. the third added S atom to the FeS_m^- cluster series results in a small decrease for the FeS_3^- cluster anion first VDE due to the formation of an S–S bond; 4. the experimental first VDEs for $Fe(SH)_{1-3}^-$ clusters are observed to increase sequentially with the addition of (SH) groups; 5. each added (SH) group to the Fe center is responsible for an increase in the first VDE of ~1.5, ~0.4, and ~0.2 eV, respectively; 6. calculated partial charge for Fe of ground state FeS_m^- (m = 1–3) cluster anions is found to increase for the first two S atoms added to Fe, but to decrease somewhat for

the third added S atom; and 7. calculated partial charges for the Fe atom of ground state $Fe(SH)_n^-$ (n = 1–3) cluster anions are found to increase with the number n of added (SH) groups. Iron sulfide/hydrosulfide mixed cluster anions are also examined. The experimental first VDE for $FeS(SH)^-$ is ~0.49 eV lower than that for FeS_2^- and is ~0.82 eV higher than that for $Fe(SH)_2^-$. Because the experimental VDE for FeS_3^- is lower than expected due to the formation of an S–S bond, the experimental first VDEs for $FeS_2(SH)^-$ and $FeS(SH)_2^-$ are close to that for FeS_3^- and are ~0.6 eV higher than that for $Fe(SH)_3^-$. These results suggest that the relative numbers of the two ligands in mixed cluster anions also affect the change in their first VDEs. The DFT calculated partial charges of the ligated Fe atom follow the trend of first VDEs for iron sulfide, hydrosulfide, and mixed sulfide/hydrosulfide cluster anions. Calculated partial charges for the Fe atom, with regard to the relative number of S atoms and (SH) groups in the considered clusters, give a qualitative understanding of, and relative estimation of, the first VDEs for these cluster anions: the higher first VDE is correlated with a higher, more positive partial charge for the Fe atom of these cluster anions. Disulfide bond (S–S) formation within the considered clusters must also be taken into account for estimating and evaluating the first VDEs of these clusters.

SUPPLEMENTARY MATERIAL

See the supplementary material for comparison of the results for $FeS_m(SH)_n^-$ [m, n = 0–3, $0 < (m + n) \leq 3$] obtained with the B3LYP and BPW91 functionals (Figure S1 and details), and other possible factors that may relate to the experimental first VDEs of these iron sulfide/hydrosulfide mixed cluster anions (Figure S2).

ACKNOWLEDGMENTS

This work is supported by a grant from the US Air Force Office of Scientific Research (AFOSR) through Grant No. FA9550-10-1-0454, the National Science Foundation (NSF) ERC for Extreme Ultraviolet Science and Technology under NSF Award No. 0310717, the Army Research Office (ARO, Grant Nos. FA9550-10-1-0454 and W911-NF13-10192), and a DoD DURIP Grant No. (W911NF-13-1-0192). We thank Dr. Zhen Zeng for help with optimization of optics associated with the PES apparatus.

[1]H. Beinert, R. H. Holm, and E. Munck, Science **277**, 653 (1997).
[2]R. Cammack, *Advances in Inorganic Chemistry* (Academic Press, New York, 1992).
[3]M. S. Nurmaganbetova, M. I. Baikenov, M. G. Meiramov, A. A. Mukhtar, A. T. Ordabaeva, and V. A. Khrupov, Pet. Chem. **41**, 26 (2001).
[4]E. Munck and E. L. Bominaar, Science **321**, 1452 (2008).
[5]D. C. Rees and J. B. Howard, Science **300**, 929 (2003).
[6]R. D. Bryant, F. V. O. Kloeke, and E. J. Laishley, Appl. Environ. Microbiol. **59**, 491 (1993).
[7]R. H. Holm, P. Kennepohl, and E. I. Solomon, Chem. Rev. **96**, 2239 (1996).
[8]S. B. Jang, L. C. Seefeldt, and J. W. Peters, Biochemistry **39**, 14745 (2000).
[9]O. Einsle, F. A. Tezcan, S. L. A. Andrade, B. Schmid, M. Yoshida, J. B. Howard, and D. C. Rees, Science **297**, 1696 (2002).
[10]T. I. Doukov, T. M. Iverson, J. Seravalli, S. W. Ragsdale, and C. L. Drennan, Science **298**, 567 (2002).
[11]J. W. Peters, W. N. Lanzilotta, B. J. Lemon, and L. C. Seefeldt, Science **282**, 1853 (1998).
[12]F. Berkovitch, Y. Nicolet, J. T. Wan, J. T. Jarrett, and C. L. Drennan, Science **303**, 76 (2004).
[13]O. A. Lukianova and S. S. David, Curr. Opin. Chem. Biol. **9**, 145 (2005).
[14]P. J. Kiley and H. Beinert, Curr. Opin. Microbiol. **6**, 181 (2003).
[15]J. A. Zuris, D. A. Halim, A. R. Conlan, E. C. Abresch, R. Nechushtai, M. L. Paddock, and P. A. Jennings, J. Am. Chem. Soc. **132**, 13120 (2010).
[16]E. N. Brown, R. Friemann, A. Karlsson, J. V. Parales, M. M.-J. Couture, L. D. Eltis, and S. Ramaswamy, JBIC, J. Biol. Inorg. Chem. **13**, 1301 (2008).
[17]L. M. Hunsicker-Wang, A. Heine, Y. Chen, E. P. Luna, T. Todaro, Y. M. Zhang, P. A. Williams, D. E. McRee, J. Hirst, C. D. Stout, and J. A. Fee, Biochemistry **42**, 7303 (2003).
[18]Y. Zu, M. M. J. Couture, D. R. J. Kolling, A. R. Crofts, L. D. Eltis, J. A. Fee, and J. Hirst, Biochemistry **42**, 12400 (2003).
[19]W. Lovenberg, *Iron-Sulfur Proteins: Biological Properties* (Academic Press, 1973).
[20]F. G. Hopkins and E. J. Morgan, Biochem. J. **32**, 611 (1938).
[21]A. D. Vinogradov, E. V. Gavrikova, and V. V. Zuevsky, Eur. J. Biochem. **63**, 365 (1976).
[22]T. A. Fedotcheva, N. L. Shimanovskii, A. G. Kruglov, V. V. Teplova, and N. I. Fedotcheva, Biochem. (Moscow) Suppl. Ser. A: Membr. Cell Biol. **6**, 92 (2012).
[23]I. S. Gostimskaya, G. Cecchini, and A. D. Vinogradov, Biochim. Biophys. Acta, Bioenerg. **1757**, 1155 (2006).
[24]R. Stern, M. DeLuca, A. H. Mehler, and W. D. McElroy, Biochemistry **5**, 126 (1966).
[25]A. T. Dinkova-Kostova, W. D. Holtzclaw, R. N. Cole, K. Itoh, N. Wakabayashi, Y. Katoh, M. Yamamoto, and P. Talalay, Proc. Natl. Acad. Sci. U. S. A. **99**, 11908 (2002).
[26]B. Mikami, K. Nomura, and Y. Morita, Biosci., Biotechnol., Biochem. **58**, 126 (1994).
[27]H. Ogino, S. Inomata, and H. Tobita, Chem. Rev. **98**, 2093 (1998).
[28]K. Koszinowski, D. Schröder, and H. Schwarz, Eur. J. Inorg. Chem. **1**, 44 (2004).
[29]K. Koszinowski, D. Schröder, H. Schwarz, R. Liyanage, and P. B. Armentrout, J. Chem. Phys. **117**, 10039 (2002).
[30]R. L. Whetten, D. M. Cox, D. J. Trevor, and A. Kaldor, J. Phys. Chem. **89**, 566 (1985).
[31]S. Yin, Z. C. Wang, and E. R. Bernstein, Phys. Chem. Chem. Phys. **15**, 4699 (2013).
[32]H. J. Zhai, B. Kiran, and L. S. Wang, J. Phys. Chem. A **107**, 2821 (2003).
[33]A. Nakajima, T. Hayase, F. Hayakawa, and K. Kaya, Chem. Phys. Lett. **280**, 381 (1997).
[34]N. Zhang, T. Hayase, H. Kawamata, K. Nakao, A. Nakajima, and K. Kaya, J. Chem. Phys. **104**, 3413 (1996).
[35]Y. J. Fu, X. Yang, X. B. Wang, and L. S. Wang, J. Phys. Chem. A **109**, 1815 (2005).
[36]Y. J. Fu, J. Laskin, and L. S. Wang, Int. J. Mass Spectrom. **263**, 260 (2007).
[37]Y. J. Fu, J. Laskin, and L. S. Wang, Int. J. Mass Spectrom. **255**, 102 (2006).
[38]X. Yang, S. Q. Niu, T. Ichiye, and L. S. Wang, J. Am. Chem. Soc. **126**, 15790 (2004).
[39]J. El Nakat, K. J. Fisher, I. G. Dance, and G. D. Willett, Inorg. Chem. **32**, 1931 (1993).
[40]L.-P. Ding, X.-Y. Kuang, P. Shao, and M.-M. Zhong, J. Alloys Compd. **573**, 133 (2013).
[41]L. Noodleman, C. Y. Peng, D. A. Case, and J. M. Mouesca, Coord. Chem. Rev. **144**, 199 (1995).
[42]J.-M. Mouesca and B. Lamotte, Coord. Chem. Rev. **178–180**, 1573 (1998).
[43]O. Hubner and J. Sauer, J. Chem. Phys. **116**, 617 (2002).
[44]O. Hubner and J. Sauer, Phys. Chem. Chem. Phys. **4**, 5234 (2002).
[45]S. Yin, Y. Xie, and E. R. Bernstein, J. Chem. Phys. **137**, 124304 (2012).
[46]S. Yin, Y. Xie, and E. R. Bernstein, J. Phys. Chem. A **115**, 10266 (2011).
[47]S. G. He, Y. Xie, F. Dong, S. Heinbuch, E. Jakubikova, J. J. Rocca, and E. R. Bernstein, J. Phys. Chem. A **112**, 11067 (2008).
[48]F. Dong, S. Heinbuch, J. J. Rocca, and E. R. Bernstein, J. Chem. Phys. **124**, 224319 (2006).
[49]O. C. Thomas, W. Zheng, and K. H. Bowen, J. Chem. Phys. **114**, 5514 (2001).
[50]K. L. Knappenberger, C. E. Jones, M. A. Sobhy, and A. W. Castleman, Rev. Sci. Instrum. **77**, 123901 (2006).
[51]L. S. Wang, H. S. Cheng, and J. W. Fan, J. Chem. Phys. **102**, 9480 (1995).
[52]O. Cheshnovsky, S. H. Yang, C. L. Pettiette, M. J. Craycraft, and R. E. Smalley, Rev. Sci. Instrum. **58**, 2131 (1987).
[53]P. Kruit and F. H. Read, J. Phys. E: Sci. Instrum. **16**, 313 (1983).

[54]G. Ganteför, K. H. Meiwes-Broer, and H. O. Lutz, Phys. Rev. A **37**, 2716 (1988).
[55]H. Wu, S. R. Desai, and L.-S. Wang, J. Phys. Chem. A **101**, 2103 (1997).
[56]C. S. Feigerle, R. R. Corderman, and W. C. Lineberger, J. Chem. Phys. **74**, 1513 (1981).
[57]M. J. Frisch, G. W. Trucks, H. B. Schlegel, G. E. Scuseria, M. A. Robb, J. R. Cheeseman, G. Scalmani, V. Barone, B. Mennucci, G. A. Petersson, H. Nakatsuji, M. Caricato, X. Li, H. P. Hratchian, A. F. Izmaylov, J. Bloino, G. Zheng, J. L. Sonnenberg, M. Hada, M. Ehara, K. Toyota, R. Fukuda, J. Hasegawa, M. Ishida, T. Nakajima, Y. Honda, O. Kitao, H. Nakai, T. Vreven, J. A. Montgomery, Jr., J. E. Peralta, F. Ogliaro, M. J. Bearpark, J. Heyd, E. N. Brothers, K. N. Kudin, V. N. Staroverov, R. Kobayashi, J. Normand, K. Raghavachari, A. P. Rendell, J. C. Burant, S. S. Iyengar, J. Tomasi, M. Cossi, N. Rega, N. J. Millam, M. Klene, J. E. Knox, J. B. Cross, V. Bakken, C. Adamo, J. Jaramillo, R. Gomperts, R. E. Stratmann, O. Yazyev, A. J. Austin, R. Cammi, C. Pomelli, J. W. Ochterski, R. L. Martin, K. Morokuma, V. G. Zakrzewski, G. A. Voth, P. Salvador, J. J. Dannenberg, S. Dapprich, A. D. Daniels, Ö. Farkas, J. B. Foresman, J. V. Ortiz, J. Cioslowski, and D. J. Fox, Gaussian 09 (Gaussian, Inc., Wallingford, CT, USA, 2009).
[58]A. D. Becke, Phys. Rev. A **38**, 3098 (1988).
[59]A. D. Becke, J. Chem. Phys. **98**, 5648 (1993).
[60]C. T. Lee, W. T. Yang, and R. G. Parr, Phys. Rev. B: Condens. Matter Mater. Phys. **37**, 785 (1988).
[61]J. P. Perdew and Y. Wang, Phys. Rev. B: Condens. Matter Mater. Phys. **45**, 13244 (1992).
[62]F. Weigend and R. Ahlrichs, Phys. Chem. Chem. Phys. **7**, 3297 (2005).
[63]V. A. Rassolov, J. A. Pople, M. A. Ratner, and T. L. Windus, J. Chem. Phys. **109**, 1223 (1998).
[64]R. Krishnan, J. S. Binkley, R. Seeger, and J. A. Pople, J. Chem. Phys. **72**, 650 (1980).
[65]W. J. Hehre, R. Ditchfield, and J. A. Pople, J. Chem. Phys. **56**, 2257 (1972).
[66]T. H. Dunning, J. Chem. Phys. **90**, 1007 (1989).
[67]Y. Xie, F. Dong, S. Heinbuch, J. J. Rocca, and E. R. Bernstein, J. Chem. Phys. **130**, 114306 (2009).
[68]C. M. Breneman and K. B. Wiberg, J. Comput. Chem. **11**, 361 (1990).
[69]A. E. Reed, R. B. Weinstock, and F. Weinhold, J. Chem. Phys. **83**, 735 (1985).
[70]J. I. Manchester, M. D. Paulsen, and R. L. Ornstein, "Modelling of biomolecular Structures and mechanisms," in *Proceedings of the Twenty-Seventh Jerusalem Symposium on Quantum Chemistry Biochemistry Held in Jerusalem, Israel*, *May 23–26 1994*, edited by A. Pullman, J. Jortner, and B. Pullman (Springer, Dordrecht, Netherlands, 1995), p. 181.
[71]D. G. Leopold and W. C. Lineberger, J. Chem. Phys. **85**, 51 (1986).
[72]X. Chen, Z. Luo, J. Li, and C. Ning, Sci. Rep. **6**, 24996 (2016).
[73]K. Siegbahn, *ESCA Applied to Free Molecules* (North-Holland Pub. Co., Amsterdam, 1969).
[74]J. Mullay, in *Electronegativity*, edited by K. D. Sen and C. K. Jørgensen (Springer, Berlin, Heidelberg, 1987), p. 1.
[75]D. W. Smith, J. Chem. Soc., Faraday Trans. **94**, 201 (1998).